Current-source 1-Ph inverter design for aircraft applications

Eralp Sener and Gurhan Ertasgin
Department of Electrical and Electronics Engineering, Faculty of Engineering, Bilecik Seyh Edebali University, Bilecik, Turkey

Abstract

Purpose – This paper aims to present an inverter with a current-source input for 400 Hz avionic systems to have a system which removes DC-link capacitors and presents a high efficiency.

Design/methodology/approach – A battery-powered DC link inductor generates a constant-current source. A single high-frequency switch is used to provide a sinusoidally modulated current before the inverter. The output of the switch is "unfolded" by a thyristor-based H-bridge inverter to generate an AC output current. The system uses a CL low-pass filter to obtain a 400 Hz pure sine wave by removing pulse width modulation components.

Findings – Simulations and Typhoon HIL real-time experiments were performed with closed-loop control to validate the proposed inverter concept while meeting the critical standards of MIL-STD-704F.

Originality/value – This current source inverter topology is suitable for avionic systems that require 400 Hz output frequency. The topology uses small DC-link inductor and eliminates bulky capacitor which determines the inverter lifetime.

Keywords Aircraft, Power electronics, Avionics, Current source inverter

Paper type Research paper

Introduction

The aviation industry makes extensive use of inverters. Inverter designs and applications may either be ground-type or plane-type, which are designed in unique ways for being used in the avionics. Aircraft make use of static inverters operating at the output frequency of 400 Hz (Sener *et al.*, 2017; Abarzadeh and Kojabadi, 2016; Yuan *et al.*, 2015). The Navy vessels have also been using this frequency for a long time (Khaligh *et al.*, 2018). Various studies have been carried out on voltage-source inverters (VSI) (Zhao *et al.*, 2014; Jiangbiao *et al.*, 2018) (Figure 1). Nonetheless, a 400 Hz current-source single-phase inverter has not been examined.

This paper presents a battery-powered 115 V 400 Hz current-source inverter (CSI) topology for aircraft applications.

Theoretical background

400 Hz systems

Size and weight are critical issues in the aviation industry, that is the reason designs satisfying the same performance with reduced volumes are more favourable in avionics applications despite their higher cost. The volume of the passive elements decreases considerably when higher AC frequency is used instead of 50 or 60 Hz. Hence, power supplies, motors, transformers and inverters also become lighter, while the length of the power transmission also decreases. Thus, following the Second World War, it has been preferred to use a frequency of 400 Hz as a standard in aircraft (Laughton and Say, 2013). Reference is made to the US Military Standard MIL-STD-704F (Table 1) to use 400 Hz voltage frequency at the power supplies in aircraft (MIL-STD-704F,2004).

Currently, non-symmetrical and non-linear loads are present in avionic systems mostly. The aircraft industry has gone through rapid growth leading to the usage of more electronic components. Therefore, loads which create harmonics are more difficult to control for higher power levels (Nouri *et al.*, 2017). Furthermore, difficulties due to the control requirements lead to the development of new control approaches. Hence, it is imperative to have higher bandwidth in non-linear and non-symmetrical load cases (Jensen *et al.*, 1998).

The use of high frequencies for energy transmission has some disadvantages. Converters with 400 Hz output are significantly sensitive to voltage drops and reactive losses which occur due to non-linear loads. These reactive losses occur because of the inductive behaviours of the leading wires or links. The conductor length and current frequency result in the mentioned losses. Higher amplitude voltage drops are observed when there is an increase in frequency. When the frequency becomes as high as 400 Hz, the reactive drops are much greater than which are observed at lower frequency range such as 50–60 Hz. These drawbacks become acceptable in exchange for smaller sizes and weights.

The skin effect creates the main resistive effect on wires. When there is an increase in frequency, the electrons normally pass through the conductor's skin instead of its core. Hence, the resistance of a conductor increases to a large extent.

The current issue and full text archive of this journal is available on Emerald Insight at: **https://www.emerald.com/insight/1748-8842.htm**

Aircraft Engineering and Aerospace Technology
92/8 (2020) 1295–1305
 [ISSN 1748-8842]
[DOI 10.1108/AEAT-10-2019-0194]

Received 2 October 2019
Revised 8 June 2020
Accepted 26 June 2020

Figure 1 Voltage-source inverter

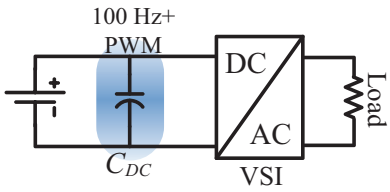

Table 1 AC normal operation characteristics for 400 Hz

Steady state characteristics	Limits
Steady state voltage	108.0 to 118.0 V, RMS
Voltage unbalance	3.0 V, RMS max
Voltage modulation	2.5 V, RMS max
Voltage phase difference	116° to 124°
Distortion factor	0.05 max
Crest factor	1.31 to 1.51
DC Component	+ 0.10 to −0.10 V
Steady state frequency	393 to 407 Hz
Peak voltage	±271.8 V

However, the losses will be minimized when shorter wires are used at 400 Hz. Furthermore, power factor (PF) problems may occur for the inverter due to the reactive, non-symmetrical and nonlinear loads of the aircraft. A power factor correction circuit or complex control systems help to solve this issue in VSIs. A CSI may also be used to solve this problem. Generally, an ideal load for a CSI presents a low impedance to harmonic currents and has a power factor close to unity. It is also very easy to connect a capacitor in parallel as a filter to resonate with and make the power factor almost unity.

Current-Source inverters

Power converters can be categorized into direct and indirect topologies for adjustable speed drives (Chong and Klug,2004; Klug and Klaassen, 2005). Furthermore, it is possible to group indirect topologies into two primary classifications: current and voltage-source converters. The classification is similar for all inverter types. VSIs use a large capacitor at the DC link, whereas CSIs use an inductor at their DC link. In previous studies made on high-power systems, it is said that CSI application is suitable for high-power applications as motor drives, induction heating or static VAr compensation (Kassakian *et al.*, 1991).

The CSIs generally emphasize a low switch count, low dv/dt switching, straightforward converter design and reliable overcurrent/short-circuit safety. The main fault is the use of large dc choke due to its limited dynamic effectiveness. In the megawatt range, high-power CSI drives are widely used (Wu *et al.*, 2008).

CSI is classified in three kinds (Vazquez *et al.*, 2009). It is shown that CSI is suggested in systems when boosting features are needed and used widely in motor drives (Daher *et al.*, 2008; Selvaraj and Rahim, 2008). This sort of converter can be categorized as pulse width modulation (PWM)-based CSIs (Joos *et al.*, 1993; Espinoza and Joos, 1997; Zmood and Holmes, 1998), load-commutated inverters (Sudhoff *et al.*, 1995) and multilevel CSIs (Antunes *et al.*, 1999).

Commonly, standard inverters categorized as CSIs can only step-up the voltage although VSIs can only step-down the voltage (Poh Chiang *et. al.*, 2005; Miaosen *et al.*, 2007). This voltage lifting ability helps to eliminate DC-DC boost circuit requirements at the DC stage of the inverter (Sajadian and Ahmadi, 2016).

VSI-based topologies replace the front end of the diode with an active front-end voltage-source converter that allows them to feed energy simply into the grid. On the contrary, current-source converters are inherently regenerative (by inversion of DC-link voltage) and do not involve modification of hardware. Also, when higher power is required, a parallel operation is possible (Wei *et al.*, 2016) and could be used in large aircraft as an additional power supply due to ease of grid connection if the aircraft has a microgrid embedded.

The reliability of the inverter is limited by the capacitors and further impeded by the possible VSI phase leg shoot-throughs. Furthermore, steep increasing and falling edges of the modulated output voltage pulse width produce high dv/dt associated electromagnetic interference noises. Due to the voltage increases resulting from these fast voltage transitions, motor insulation degradation causes high-frequency losses in the windings and electric motor cores and generates bearing-leakage currents that are harmful to the life span of the bearings. Furthermore, the VSI requires a bidirectional buck-boost converter to operate from a low-voltage battery and is used in some of the hybrid electric vehicles (HEV) currently on the market (Muta *et al.*,2004; Nozawa *et al.*, 2009; Su and Tang, 2011).

Additionally, the CSIs are less studied and implemented compared to VSIs, partially due to reverse blocking of the CSIs switches. If IGBTs are used for the CSIs, then only diodes linked to the IGBTs can achieve the reverse blocking function. This results in a quite large semiconductor loss during the conduction time. The newly founded RB-IGBT is characterized by symmetrical blocking voltage. In its off state, it can block both forward and reverse voltages (Takei *et al.*, 2004; Motto *et al.*,2004). Improving semiconductor switches has made CSIs more interesting in several applications, such as uninterrupted power supplies, ac drives and reactive power compensators owing to their inherent short-circuit protection performance, robustness and direct current control capability (Wu *et al.*, 2008; Zmood and Holmes, 2001). The current-source topology based on thyristor offers a considerably better output for very high-power systems thanks to the low-voltage drop of the semiconductors used (Wiechmann *et al.*, 2008). Also, for low power applications as the proposed inverter, low-voltage drop and high efficiency are important and less switching loss improves the efficiency of the circuit.

It is analysed that the energy storage element is needed by single-phase inverters at the DC link due to the lack of internal energy storage in the inverter output stage. Single-phase VSIs are usually preferred in the industrial applications due to their size and weight benefits as they store energy with capacitors at the DC link (Figure 1). Furthermore, different industrial applications require the use of VSIs as voltage-source. Single-phase CSIs are not preferred due to their less energy storage capacity as such inductors cannot store energy as much as

capacitors as they need substantially higher volume for the same amount of energy storage capacity. Hence, they are unable to decrease double line frequency voltage or current variations less than acceptable levels unless they are quite bulky. For a 50/60 Hz system, double line 100 Hz ripples in the DC link is inevitable. A current source-inverter block diagram having a big DC link inductor is depicted in Figure 2. This inductor at the DC link makes the inverter current-source and provides energy storage for the fluctuations. The DC link inductor has a smaller volume in this paper because of the 400 Hz output frequency. Then the ripples at the DC link will be 800 Hz and the energy storage requirement for the DC link will be much lower compared to a 50 Hz line frequency.

Energy storage elements at the DC link is always an issue especially for CSIs due to their volume. Therefore, the reduction of the energy storage requirement so the size of the component is critical. A modulation method with a resonant filter was studied by Alajmi *et al.* to decrease the ripples at the DC link of the inverter (Alajmi *et al.*, 2012). There is a decrease in efficiency due to power reduction because of ripples. In the previous studies, another method was implemented as an active buffering technique to decrease the DC link inductor size (Cossutta *et al.*, 2015; Ohnuma *et al.*, 2014). This method increases the number of components increasing circuit volume which may lead to reliability issues with further losses. Li, R *et al.* also examine an active modulation approach to decrease the size of the inductor (Li *et al.*, 2006). Even though losses are decreased by a modulation method using zero current switching (ZCS) method having an active buffer system, the control complexity is increased (Watanabe and Itoh, 2015). Although the aim of these designs is primarily to have constant current at the DC link, mentioned disadvantages are critical for the systems which have grid frequency (50/60 Hz).

There is an increase in the size concerning the DC link inductor when the ripple frequency is reduced. As a result, an inverter system that has higher frequency fluctuations at the DC link was implemented. Although 800 Hz fluctuations are present in the DC link as a result of the single-phase inverter output, the required DC link inductor is substantially smaller in size and weight as less energy required to attenuate the low-frequency ripples. Hence, when a high output frequency is selected, an inductor which has eight times reduced inductance will be sufficient compared to the 50 Hz systems. This can be seen below equations clearly.

$$X_L = 2\pi f_1 L_1 = 2\pi f_2 L_2 \tag{1}$$

Figure 2 Current-source inverter

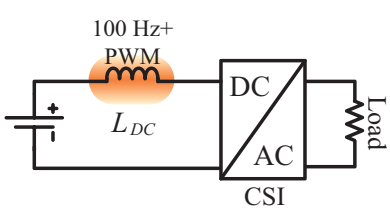

$$f_1 = 8f_2 \tag{2}$$

$$L_1/8 = L_2 \tag{3}$$

Consequently, VSIs can be replaced with CSIs in the avionics industry. CSIs have certain advantages compared to VSIs as shown in (Laughton and Say, 2013; Ertasgin *et al.*, 2013):

- DC-Link capacitors with less reliability and shorter lifetime are changed with reliable and robust inductors;
- Simpler current control;
- Easy to meet power factor requirements;
- No need for feedback diodes;
- Short-circuit protection is naturally included;
- Higher mechanical fault tolerance without a DC link capacitor.

This paper mainly studied to provide a 400 Hz sinusoidal output using the topology in Figure 3. It should be noted that here CSIs are seen less preferable due to their resistive and core losses in the DC link. The size reduction owing to 400 Hz output frequency requirement helps to have less core and resistive losses. Many researchers also proposed a soft-switching technique to deal with these losses (Ohnuma *et al.*, 2014),(Mishima *et al.*, 2012),(Shalini and Dhanalakshmi, 2017). The proposed topology has ZCS as H-bridge circuit consists of thyristors which have natural turn-off capability due to the waveshaper (WS) output current as the current falls below the thyristor minimum holding current.

Proposed topology

A similar version of the proposed topology was implemented as a grid-connected PV inverter (Ertasgin *et al.*, 2013). The previous topology includes a bulky inductor at the DC link and a diode after the high-frequency switch. However, the new CSI topology demonstrated in Figure 3 consists of a smaller inductor to supply a constant current-source by using a battery. Then a switch is used for high-frequency switching to shape the current with sinusoidal PWM. The new topology does not have a diode after the high-frequency switch. A thyristor-based bridge unfolds (reverses the polarity) the PWM chopped

Figure 3 Proposed CSI topology

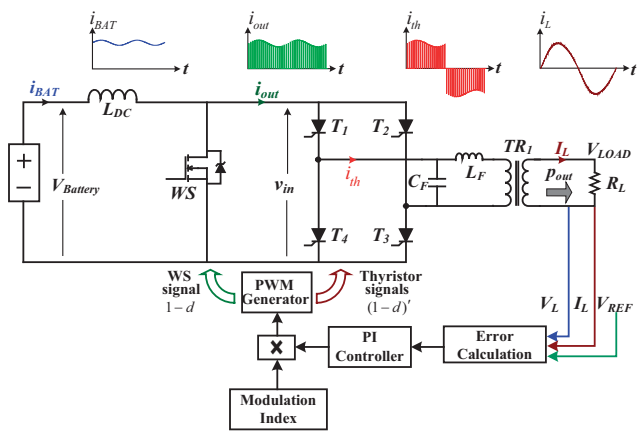

waveform before a capacitive-inductive (CL) low-pass filter to generate a sine wave.

There are certain advantages of the CSI topology:

- Smaller switching loss because of single switch modulation, which also leads to ZCS for thyristors.
- Wave-shaped current approaches zero sinusoidally due to thyristors nature. There is no crossover distortion and hence this does not result in a harmonic generation.
- The overall inverter efficiency depends on the number of switching elements. Therefore, fewer components used in the current path. For example, no diode is present in series with the thyristor to prevent the reverse voltages. In addition, there is no further commutation circuit for thyristors owing to a single MOSFET switch which commutes them actively.

Fundamental analysis

Figure 3 shows the idealised circuit of the CSI with the input and output currents. The idealised model omits losses such as DC link inductor without copper and iron losses and switches have no on-resistance and switching losses. The waveshaper switch has high frequency switching capability. Two controlled sources are used using the output voltage (4) and current (5) correlations to model the WS. This removes the PWM switching effects and CSI can create a pure sinewave output with no low-pass filter requirement.

The output current i_{OUT} is the complement of the PWM duty-cycle (control signal) d as indicated by (4). The output of WS can be obtained by the product of (1-d) and input current i_{IN} based on the controlled current-source as seen in Figure 4.

$$i_{OUT} = i_{IN}(1 - d) \tag{4}$$

$$v_{IN} = v_{OUT}(1 - d) \tag{5}$$

The relationship between the duty cycle and the modulation index m_A is shown in equation (6) below.

$$1 - d = m_A|\sin\theta| \tag{6}$$

Similarly, the controlled voltage-source sets the output voltage (V_{OUT}) as the (1-d) multiplication of the input voltage (V_{IN}). Therefore, a DC output current which is full-wave rectified is created for the unfolding circuit ignoring the PWM as seen in Figure 4. Then the unfolding circuit reverses the polarity of the DC. Finally, a pure sinusoidal waveform is created. This ideal model shows the fundamental operation of the CSI without losses and an output filter.

Figure 4 Equivalent circuit diagram of ideal single-phase CSI diagram showing ideal waveforms

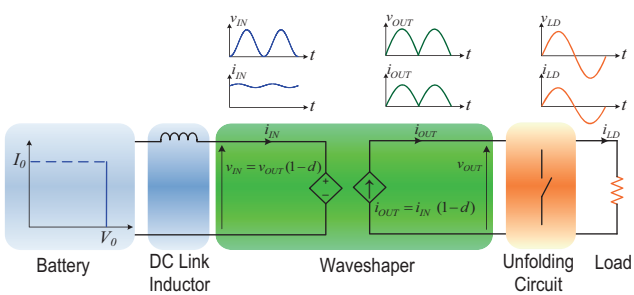

Fundamental operation of the current-source inverter

Figure 5 depicts the flow diagram of the current source inverter showing current and voltage waveforms starting from the load employing a battery model. When the load voltage v_{LD} is provided as:

$$v_{LD} = V_{PK}\sin(\omega t) \tag{7}$$

where V_{PK} and ω are the peak value of the load voltage and angular frequency, respectively. The WS output voltage v_{OUT} equals the absolute value of the load voltage:

$$v_{OUT} = V_{PK}|\sin(\omega t)| \tag{8}$$

Combining the WS voltage transfer equation (5) and the duty ratio equation (6), the following statement is made for the WS input voltage $v_{IN}(t)$:

$$v_{IN}(t) = V_{PK}\, m_A \sin(2\,\omega t) = V_{PK}\, m_A 0.5\,[1 - \cos(2\,\omega t)] \tag{9}$$

The WS input voltage as a sine wave with a DC offset has a frequency which is twice the line frequency. Therefore, the average battery output voltage and the waveshaper input voltage should be the same because the inductor DC voltage drop is zero. Thus, the average battery output voltage v_{BT} equation is as follows:

$$v_{BT} = \overline{v_{IN}(t)} = \frac{1}{2} V_{PK} m_A \tag{10}$$

The characteristics of the battery and the DC link inductance value determine the resultant battery output current, i_{BT} corresponds to the WS input voltage in equation (10). Generally, there will be some components with double line frequency. The WS input current i_{IN} is the same as the battery output current. The WS output current, i_{OUT}, is a modulated version of the input current is given by equation (4). Eventually, the load current i_{LD} is an unfolded form of the WS output current.

DC link inductor sizing

A single-phase inverter produces output power which fluctuates at 800 Hz, ($\sin^2\omega$t), and as the battery provides constant power (current and voltage), an energy storage element, such as an inductor, is required. The inductor provides constant current and the necessary energy storage to deliver the inverter 800 Hz pulsating power. The inductor is analogous to the input capacitor in a VSI.

The difference between the battery output power and instantaneous inverter input power flows through this inductor and yields an 800 Hz current ripple from the battery. These ripples ($\Delta i_L = I_{max} - I_{min}$) can be reduced with the appropriate inductor selection. The procedure to select the appropriate inductance value is given below equations (11)-(14). If the average power delivered by the battery is given as:

Figure 5 CSI ideal waveform flow diagram starting from the load voltage to obtain sinusoidal output current

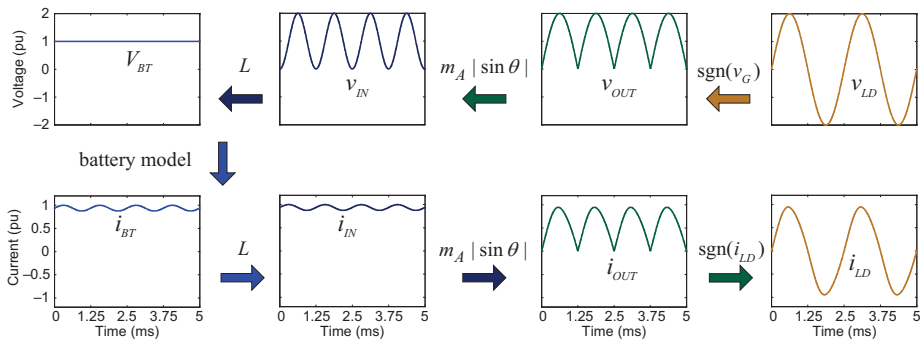

$$P_{AVG} = P_{BT} \tag{11}$$

The input power for the full-bridge inverter P_{IN} is the sum of the instantaneous power and the battery output power P_{BT} as seen below:

$$P_{IN} = P_{AVG} + P_{AVG}\,sin(2\pi 800t) \tag{12}$$

Then the integration of $P_{BT} - P_{IN}$ will give the stored inductor energy:

$$\Delta E = \int (P_{BT} - P_{IN})\,dt = P_{AVG}K \tag{13}$$

where ΔE is the energy which must be stored by the inductor temporarily. K is an integral constant and L is the inductance. Equalising inductor energy E and ΔE will determine the appropriate inductor value.

$$E = \frac{1}{2}\left(I_{max}^2 - I_{\min}^2\right) \Rightarrow L = \frac{2P_{AVG}K}{I_{max}^2 - I_{\min}^2} \tag{14}$$

Current waveshaping

As seen in Figures 3 and 4, the current waveshaper MOSFET transforms the DC into a PWM chopped current that resembles the rectified sine wave. The WS switch uses sinusoidal PWM to shape the DC link current to obtain a rectified 400 Hz sine wave which requires unfolding to generate a sine wave shape subsequently a low-pass filter. The bridge thyristors are switched to reverse the polarity of the second cycle of the sinusoidally modulated waveform. The unfolding circuit output current is filtered by a second-order CL type low-pass output filter. To simply describe the working principle of the inverter, main waveshapes and wave shaping circuit is displayed in Figure 6.

Please note that, despite the similarities with conventional two-stage inverter with a boost converter and a sinusoidal PWM controlled H-bridge inverter, this topology does not operate in voltage boost mode, it operates as a current waveshaper with a bridge unfolding circuit. The H-bridge inverter is acting as a simple square wave inverter to unfold the current. Therefore, the topology has fewer components with less switching losses and requires a smaller heatsink.

Figure 6 Waveshaping process of the CSI

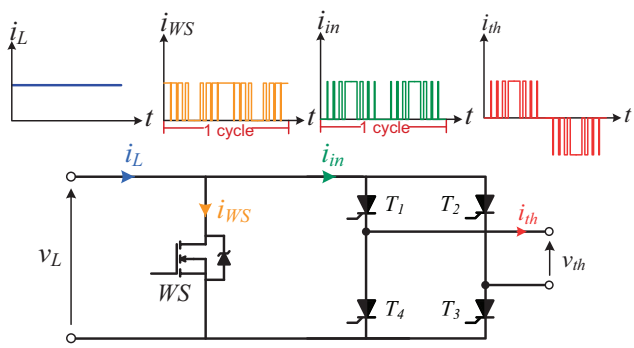

Control design

Stabilizing the voltage output for high-quality waveform is required in avionic systems. There are various methods to control inverters. These control approaches are classified into two groups according to the control structure to meet some of the requirements. One is the single loop voltage control (Wang *et al.*, 2017; Wang *et al.*, 2015) and the other is the double loop voltage control (Wang *et al.*, 2013; Wang *et al.*, 2015). Figure 7 shows the control algorithm which uses a double loop controller. A PI controller with voltage and current feedbacks are added to the circuit. As a design matter, RMS values of the output voltage and output current is obtained to apply a PI controller suitable for DC systems. For the sake of simplicity, complex AC control methodologies were avoided.

Reference value $r(s)$ is given to the positive input of the subtractor as unit function. The measured output voltage normalized by dividing the measured value to the required voltage value. Then the obtained value is transferred to the negative input of the subtractor. The error function $e(s)$ is obtained by this subtraction. A PI controller is used to calculate

Figure 7 Proposed control design

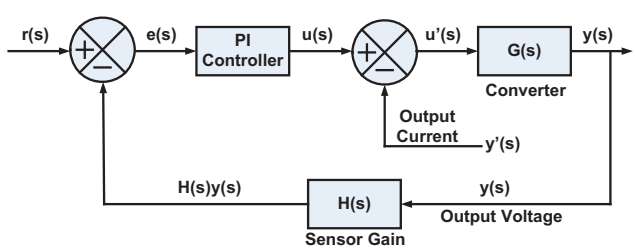

the control signal u(s). The feedback value which is a load current variation is taken from the current output. The obtained current value is subtracted from u(s) to obtain a secondary feedback loop for a more stable system. Before the gating signal generation stage, u′(t) is converted to (1 − u′(t)). This conversion enables the controller to obtain a better settling time. The inverted control signal generates a better response due to the modulated (1-d) switch input.

PI variables are first tuned by Ziegler–Nichols heuristic tuning method (Valério and Da Costa, 2006). After the variables obtained, fine-tuning is accomplished for voltage feedback control. To increase stability, a second control loop which is a current feedback loop is added to the control system. Second loop required a minor tuning for the PI controller too. As a result, the gain is selected as 0.025 and time constant is selected as 0.002 s.

System simulation

Simulation of the inverter

PSIM is used for inverter system simulation as seen in Figure 8. 1.2 V is added to thyristor parameters as a forward voltage drop. Low-pass output filter capacitor's ESR and inductor's resistor are assumed 0.01 Ω to acquire better efficiency prediction initially.

115 V RMS output voltage and 400 Hz frequency requirements for aircraft power system application are carefully considered for the design of the 400 Hz power inverter. An ideal output transformer is used to obtain 115 V RMS. The output transformer is used to increase the voltage level and provide isolation. Figure 8 also shows control blocks of the simulation. Logic elements, comparators and signal sources are used to create required triggering pulses. PI control was used to initially confirm the 400 Hz CSI.

Table 2 provides the simulation parameters of the CSI topology. In this table, the simulated system meets the output voltage, total harmonic distortion (THD) and crest factor requirements with respect to the (MIL-STD-704F,2004).

CSI waveforms are depicted in Figure 9. DC link current fluctuations as 800 Hz can be seen in the top figure as 0.3 A peak-to-peak. Please note that the ripple has the same frequency with the output power. The single-phase oscillations

Figure 8 Simulation circuit of the proposed topology with closed-loop control

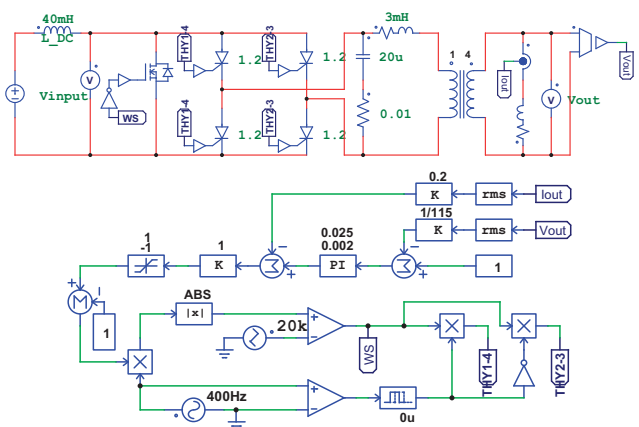

Table 2 Simulation parameters of the CSI

Parameter	Value
Input voltage (V_{OC})	28 V
Input current (I_{OC})	4.5 A
Output power (P_{OUT})	120.75 W
Output voltage (V_{OUT})	115 V RMS
Output current (I_{OUT})	1.05 A RMS
Crest factor	1.43
THD	2.74%

Figure 9 Simulation output of the current at the DC link, output current, output voltage and output power of the inverter (top to bottom)

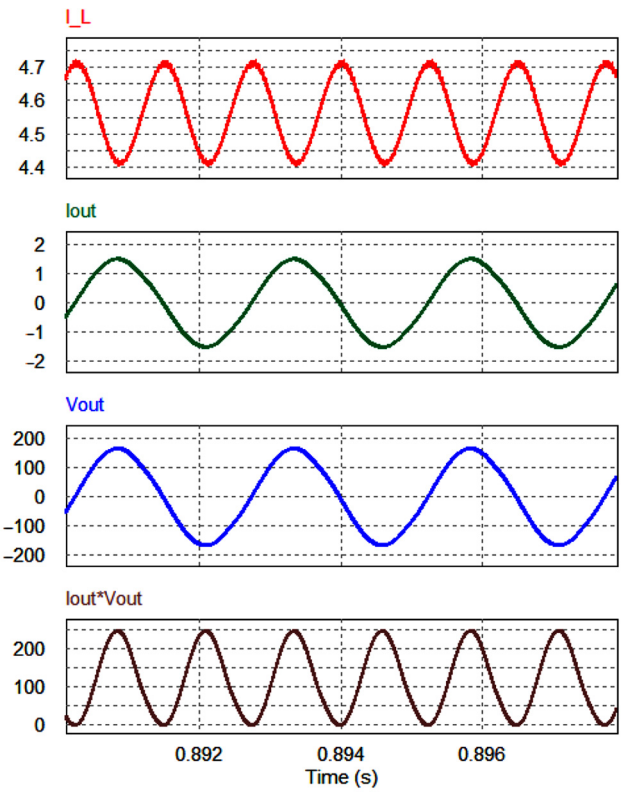

of the output power result in DC link current and voltage fluctuations. The obtained distortion value is 2.74%. This value meets the THD requirements as it is below the maximum allowable THD which is 5% (MIL-STD-704F,2004). As seen from the figures the power factor is 0.999 which can be assumed as unity.

The control studies show that different tests are made for the control system robustness. These PSIM simulations include resistive load tests which are accomplished at the range of 70 to 150 Ω. Tests are done for observing the real power (W) limits and settling time of the control system and the circuit. Table 3 shows Settling Time (ST), which is the time required for the system to reach steady-state, PF and THD results for the resistive load cases. PF does not show considerable change due to resistive load. THD is measured from the output voltage as current and voltage provide almost the same THD values.

Table 3 Resistive load test

Load	%THD	ST
70 Ω	9.97	0.155 *s*
90 Ω	8.15	0.120 *s*
110 Ω	2.74	0.093 *s*
130 Ω	0.75	0.026 *s*
150 Ω	0.60	0.013 *s*

The resistive test results show that increasing load causes a reduction in both THD and ST. The circuit with this control system can be implemented for lower power applications. However, decreasing load causes an increment at both THD and ST. Therefore, the circuit is designed for 120 W, higher power requirements do not cause serious malfunctions. The THD results obtained at higher power levels are not meet MIL-STD 704 F standards however the system is still operational at 150% power and ST is acceptable.

Following the resistive load test, inductive load cases are carried out. Table 4 shows different inductive load cases from 4 to 20 mH. 110 Ω resistive load, which is the design point, is kept constant at the output.

The inductive load test shows the THD difference between the output voltage and output current. Also, PF change occurs with the increasing load. However, settling time is not affected by changing the inductive load. Therefore, the THD difference increases with the inductive load increment. This difference caused by the sum of the negative effect of the increased load and current filtering ability of inductor. It is seen that PF increases by reactive power increment.

Low-pass filter design

The output current of the inverter contains (high) frequency harmonics due to PWM switching. To meet the required harmonics standards, they must be filtered with a low pass filter at the output of the unfolding circuit. VSIs generally use a second-order LC filter or a third-order LCL filter with an addition of L. However, CSIs use a second-order CL filter based on the filter mismatch criteria (Nave, 1991). As seen in equation (15), the filter cutoff (or resonant) frequency rely on the frequency-dependent components such as inductance and capacitance. The filter quality factor is critical when selecting the component values for the inductor and capacitor. It is recommended to select a quality factor between 2 and 4 for a low-pass filter design (Nave, 1991).

$$f_C = \frac{1}{2\pi\sqrt{LC}} \tag{15}$$

Table 4 Inductive load test

Load	%THD (V)	%THD (I)	ST	PF
4 mH	6.21	5.98	0.103 *s*	0.995
8 mH	6.45	5.63	0.109 *s*	0.983
12 mH	6.83	5.28	0.109 *s*	0.963
16 mH	9.07	6.18	0.109 *s*	0.937
20 mH	9.27	5.69	0.109 *s*	0.907

These MIL-STD 704 F requirements are taken into account when designing the low-pass filter for the CSI:

- have 5% or less THD by removing high-frequency harmonic content from the inverter output current; and
- to be operational within the defined 108 to 118 V RMS voltage and 393 to 404 Hz frequency range.

Experimental results

In this study, the hardware experimental work is conducted on a Typhoon HIL-402 module. The hardware-in-the-loop (HIL) processor includes practically all the elements to do measurements. The defined controller can work in real-time, with 20 ns PWM resolution, in a closed-loop update rate of 1 MHz with high accuracy for each stage of a converter system. Figure 10 illustrates the power stages of the CSI which were designed with the support of the Typhoon HIL Schematic Editor. This enables to use the required power electronics components. The circuit design can be compiled and executed to see the model and controller performance. An integrated mixed-signal oscilloscope monitors the execution of control centre test scenarios and automates the verification process with Python scripts (Typhoon HIL, 2019).

As shown in Figure 10, control blocks in the HIL environment are primarily used without a connection to a physical controller. A voltage source provides 28 V DC for the inverter. The DC link inductor L1 is used before the waveshaper as a buffer. DC voltage source and inductor model a current source. IGBT as a high-frequency switch was the only choice in the HIL and used as WS. Before the low-pass filter, the thyristor-based bridge inverter is used to unfold the sinusoidally chopped unipolar 400 Hz waveform into a bipolar waveform. Complimentary pulses control thyristors. They receive the compliment pulses of the WS (Figure 3). Thyristors turn-off naturally due to the

Figure 10 The proposed topology design with control using the HIL software

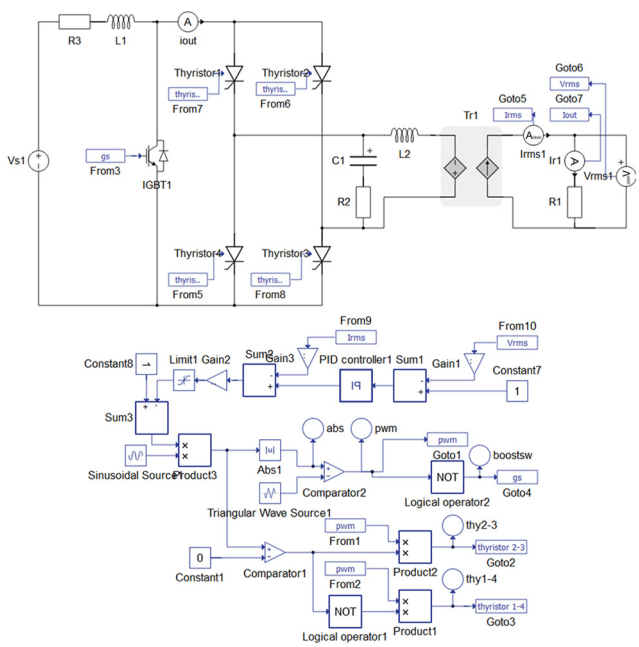

nature of the WS output current, i.e. the current properly falls below the thyristor holding current to turn them off. When T1 and T3 switches are conducting simultaneously a positive output current is generated and when T2 – T4 pairs is conducting a negative output current is obtained. The CL filter with ESR resistor is realized after the unfolding circuit. Then an ideal transformer is used to achieve 115 V output. It is also critical to mention that the transformer could cause extra losses however it provides isolation.

The inverter control stage is designed using the signal processing tool of the Typhoon HIL Schematic Editor. Compared to the triangular wave, the absolute value of the 400 Hz sine wave creates pulses that produce rectified sine waves. The output is inverted to drive the IGBT switch. The variations of the same PWM pulses were used for thyristor switching. Figure 11 shows the control signals for the unfolding process. In this stage, thyristors are triggered by comparing the sine wave with zero to activate positive and negative current cycles. Typhoon HIL SCADA generates these signals. The thyristor signals are complementary to the waveshaper triggering signals as can be seen in Figure 11. The FPGA processor is used by internal modulators which enables rapid and appropriate modulation signals.

Component blocks and signal processing blocks are used from the Typhoon HIL Schematic editor library during the HIL testing phase. Figure 11 shows the control signals which are produced by the control stage of the modulation given in Figure 10. Modulation elements involve reference sine wave and rectified sine wave. GS output controls the IGBT switch which uses the sinusoidal PWM and shapes the waveform. The outputs of PWM 2–3 and PWM 1–4 are triggering thyristors 2–3 and 1–4, respectively.

The rectified sine wave is connected to GS and for IGBT switching the reverse output signal is used. Compared to '0' the reference sinusoid separates positive and negative areas of the sine wave. Positive and negative signals are linked as 1–4 and 2–3 to thyristor PWM blocks.

Test procedure

400 Hz 115 V inverter tested with the Typhoon HIL 402. To avoid audible switching noise and to use smaller low-pass output filter, 20 kHz was selected as switching frequency for the WS switch. As previously stated, thyristors have a voltage drop of 1.2 V. The rest of the inverter circuit was assumed ideal during measurements.

Figure 12 depicts the input and output waveforms of the inverter system. Figures at the left corner show the output voltage and current waveforms using a resistive load. The top right corner is the DC link inductor current. 0.2 A peak-to-peak ripple current corresponds to 3.7%. This value met the requirements for the allowable current ripple (MIL-STD-704F,2004). The power waveform is seen at the bottom right corner in Figure 12. The obtained efficiency is around 97% due to mainly ideal circuit application. The output transformer, DC link inductor and waveshaper switch will yield more losses if the system constructed. However, optimizations and better component selections in-circuit production may allow achieving that efficiency at the rated power.

Experimental results were analysed using MATLAB. Table 5 shows the model parameters of the designed CSI. HIL measurements are very similar to the simulations.

The FFT analysis of the output current is seen in Figure 13. The output current THD value of 2.17% is approximately 0.5% lower as compared to the simulated value of 2.73%. This could be due to some assumptions as sampling period, ideal capacitive and inductive elements without any resistance in the simulation software. However, both values are below the maximum allowable THD value which is 0.05%, indicated at

Figure 11 The waveshaper switch and thyristor signals from Typhoon HIL® Signal Processing Blocks

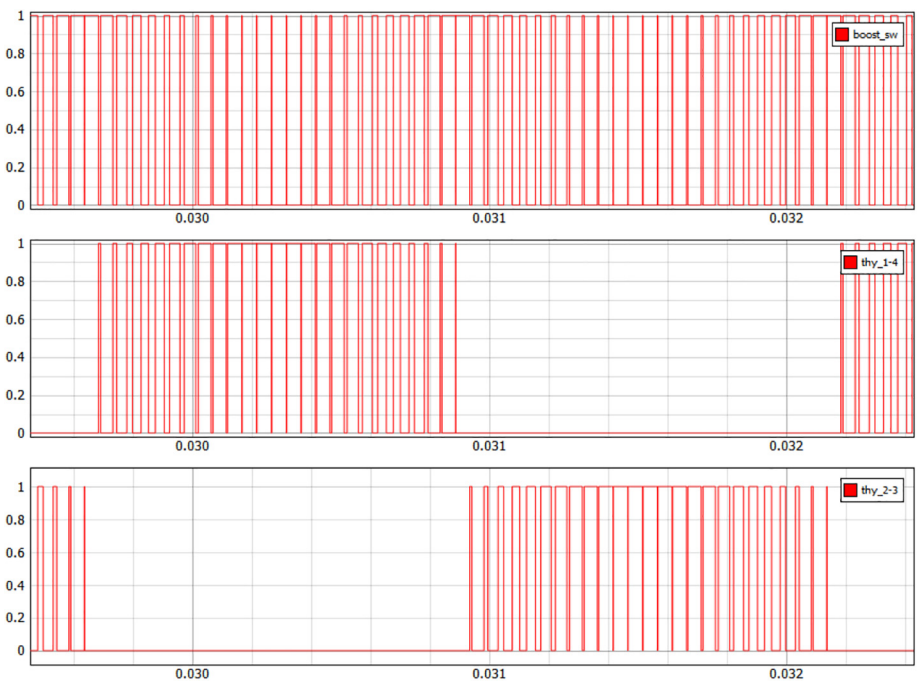

Figure 12 Inverter output values shown in Typhoon HIL SCADA

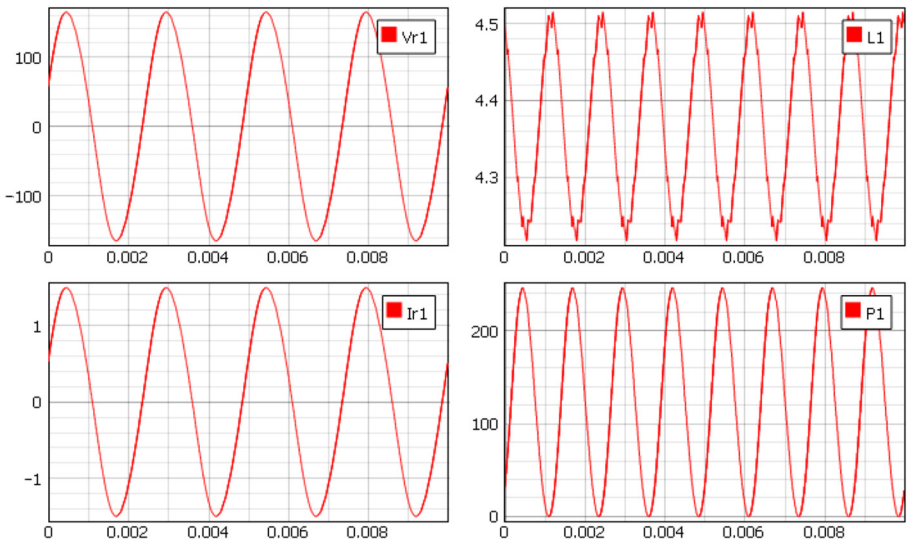

Notes: Top left corner is the output voltage (V), top right corner is DC-link current (A), bottom left corner is the inverter output current (A) and bottom right corner is the output power (W).

Table 5 Proposed 400 Hz CSI parameters

Variables	Results
Output voltage (V_{OUT})	115 V
Output current (I_{OUT})	1.05 A
Frequency (Hz)	400 Hz
Crest factor	1.43
Output power (P)	120 W
THD (%)	2.17

Figure 13 FFT analysis results of the current output obtained from Typhoon HIL Test

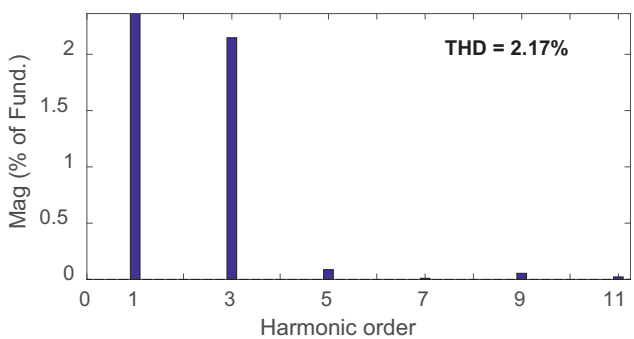

the standards (MIL-STD-704F,2004). Designed filter and/or control algorithm optimizations can further reduce the THD.

Figure 14 shows the power factor curve as a function of inverter output power as simulation and measurement. The figure proves that the requirements for the power factor have been met (MIL-STD-704F,2004). It also depicts both simulations and test measurements have a good agreement.

Figure 14 Simulated and measured power factor vs output power

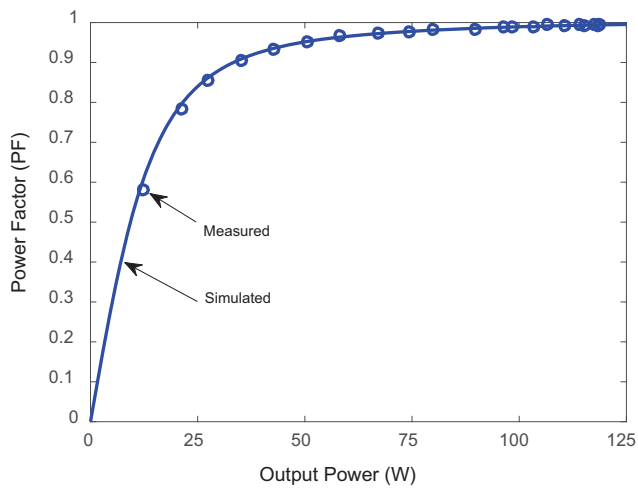

Conclusion

This study shows the simulation and validation of the 400 Hz CSI for avionic systems by using HIL system. A significantly small DC-link inductor can be used for a CSI due to the nature of 400 Hz systems, without a requirement for complex control techniques. DC link capacitors especially electrolytic ones are a major issue for VSIs as they determine the lifetime of the inverter and reduce high-temperature operation capability. Hence CSI topology ignores these kinds of problems. This topology uses the minimum number of components with a single high-frequency switch while allowing thyristor-based H-bridge for ZCS as the current adequately falls below the thyristor holding current to turn them off. This also prevents

crossover distortion. Therefore, higher reliability and efficiency can be obtained.

Instead of testing the system with different loads, only a resistive load is used to observe the performance of the proposed CSI system solely. With this approach, THD and PF requirements of MIL-STD704F compliancy has been satisfied by the presented topology independent of the load effect. Although different loads have not been tested, THD and power factor requirements were met with the closed-loop control. The limits of the closed-loop control system and the robustness is tested through PSIM simulation using different resistive and inductive loads.

The smaller DC link inductor does not degrade the dynamic performance of the inverter as more time is not required for the load current to change in response to a control command. To conclude, this topology is a very promising candidate for aviation applications by using fewer components and eliminating electrolytic capacitors. This leads to a smaller size, less weight, reduced converter cost and better efficiency.

References

Abarzadeh, M. and Kojabadi, H.M. (2016), "A static ground power unit based on the improved hybrid active neutral-point-clamped converter", *IEEE Transactions on Industrial Electronics*, Vol. 63 No. 12, pp. 7792-7803.

Alajmi, B.N., Ahmed, K.H., Adam, G.P. and Williams, B.W. (2012), "Single-phase single-stage transformerless grid-connected PV system", *IEEE Transactions on Power Electronics*, Vol. 28 No. 6, pp. 2664-2676.

Antunes, F.L., Braga, H.A.C. and Barbi, I. (1999), "Application of a generalized current multilevel cell to current-source inverters", *IEEE Transactions on Industrial Electronics*, Vol. 46 No. 1, pp. 31-38.

Chong, K.J. and Klug, R.D. (2004), "High power medium voltage drives", *2004 International Conference on Power System Technology, 2004. PowerCon 2004*, Vol. 1, *IEEE*, pp. 658-664.

Cossutta, P., Aguirre, M.P., Cao, A., Raffo, S. and Valla, M.I. (2015), "A novel modulation technique for single phase current source inverters with active buffering", *2015 IEEE International Conference on Industrial Technology (ICIT)*, *IEEE*, pp. 2036-2041.

Daher, S., Schmid, J. and Antunes, F.L. (2008), "Multilevel inverter topologies for stand-alone PV systems", *IEEE Transactions on Industrial Electronics*, Vol. 55 No. 7, pp. 2703-2712.

Ertasgin, G., Soong, W.L. and Ertugrul, N. (2013), "Analysis and design of single-phase current-source grid-connected PV inverter", *2013 15th European Conference on Power Electronics and Applications (EPE)*, *IEEE*, pp. 1-10.

Espinoza, J.R. and Joos, G. (1997), "Current-source converter on-line pattern generator switching frequency minimization", *IEEE Transactions on Industrial Electronics*, Vol. 44 No. 2, pp. 198-206.

Jensen, U.B., Rasmussen, M.P., Mortensen, T., Blaabjerg, F. and Pedersen, J.K. (1998), "A new control method for 400 Hz ground power units for airplanes", *Conference Record of 1998 IEEE Industry Applications Conference. Thirty-Third IAS Annual Meeting (Cat. No. 98CH36242)*, Vol. 2, *IEEE*, pp. 1469-1476.

Joos, G., Moschopoulos, G. and Ziogas, P.D. (1993), "A high performance current source inverter", *IEEE Transactions on Power Electronics*, Vol. 8 No. 4, pp. 571-579.

Kassakian, J.G., Schlecht, M.F. and Verghese, G.C. (1991), *Principles of Power Electronics*, Pearson.

Khaligh, H., Torkaman, H. and Ebrahimian, A. (2018), "Novel algorithm for optimum output passive filter design in 400 Hz inverter", *2018 9th Annual Power Electronics, Drives Systems and Technologies Conference (PEDSTC)*, *IEEE*, pp. 335-340.

Klug, R.D. and Klaassen, N. (2005), "High power medium voltage drives-innovations, portfolio, trends", *2005 European Conference on Power Electronics and Applications*, *IEEE*, p. 10.

Laughton, M.A. and Say, M.G. (Eds) (2013), *Electrical Engineer's Reference Book*, Elsevier.

Li, R.T., Chung, H.S. and Chan, T.K. (2006), "An active modulation technique for single-phase grid-connected CSI", *2006 37th IEEE Power Electronics Specialists Conference*, *IEEE*, pp. 1-7.

MIL-STD-704F (2004), "Aircraft electric power characteristics", Department of Defense Interface Standard (MIL-STD-704F).

Mishima, T., Takeuchi, Y. and Nakaoka, M. (2012), "Analysis, design, and performance evaluations of an edge-resonant switched capacitor cell-assisted soft-switching PWM boost dc–dc converter and its interleaved topology", *IEEE Transactions on Power Electronics*, Vol. 28 No. 7, pp. 3363-3378.

Motto, E.R., Donlon, J.F., Tabata, M., Takahashi, H., Yu, Y. and Majumdar, G. (2004), October. "Application characteristics of an experimental RB-IGBT (reverse blocking IGBT) module", *Conference Record of the 2004 IEEE Industry Applications Conference, 2004. 39th IAS Annual Meeting*, Vol. 3, *IEEE*, pp. 1540-1544.

Muta, K., Yamazaki, M. and Tokieda, J. 2004. "Development of new-generation hybrid system THS II-Drastic improvement of power performance and fuel economy (no. 2004-01-0064)", SAE Technical Paper.

Nave, M.J. (1991), *Power Line Filter Design for Switched-Mode Power Supplies*, Van Nostrand Reinhold, New York, NY,

Nouri, M., Salari, O., Hashtrudi-Zaad, K. and Bakhshai, A. (2017), "A hybrid designed digital dual-loop control of high power ground power unit (GPU)", *2017 19th European Conference on Power Electronics and Applications (EPE'17 ECCE Europe)*, *IEEE*, p. P-1.

Nozawa, N., Maekawa, T., Nozawa, S. and Asakura, K. (2009), "Development of power control unit for compact-class vehicle", *SAE International Journal of Passenger Cars – Electronic and Electrical Systems*, Vol. 2 No. 1, pp. 376-382.

Ohnuma, Y., Orikawa, K. and Itoh, J.I. (2014), "A single-phase current-source PV inverter with power decoupling capability using an active buffer", *IEEE Transactions on Industry Applications*, Vol. 51 No. 1, pp. 531-538.

Sajadian, S. and Ahmadi, R. (2016), "Model predictive-based maximum power point tracking for grid-tied photovoltaic applications using a Z-source inverter", *IEEE Transactions on Power Electronics*, Vol. 31 No. 11, pp. 7611-7620.

Selvaraj, J. and Rahim, N.A. (2008), "Multilevel inverter for grid-connected PV system employing digital PI controller", *IEEE Transactions on Industrial Electronics*, Vol. 56 No. 1, pp. 149-158.

Sener, E., Ertasgin, G. and Zuber, D. (2017), "Design of a 400 Hz current-source single-phase converter for avionic systems", *2017 IEEE Vehicle Power and Propulsion Conference (VPPC)*, *IEEE*, pp. 1-6.

Su, G.J. and Tang, L. (2011), "Current source inverter based traction drive for EV battery charging applications", *2011 IEEE Vehicle Power and Propulsion Conference*, *IEEE*, pp. 1-6.

Sudhoff, S.D., Zivi, E.L. and Collins, T.D. (1995), "Start up performance of load-commutated inverter fed synchronous machine drives", *IEEE Transactions on Energy Conversion*, Vol. 10 No. 2, pp. 268-274.

Takei, M., Naito, T. and Ueno, K. (2004), "Reverse blocking IGBT for matrix converter with ultra-thin wafer technology", *IEE Proceedings – Circuits, Devices and Systems*, Vol. 151 No. 3, pp. 243-247.

Typhoon HIL (2019), available at: www.typhoon-hil.com (accessed 17 January 2019).

Valério, D. and Da Costa, J.S. (2006), "Tuning of fractional PID controllers with Ziegler–Nichols-type rules", *Signal Processing*, Vol. 86 No. 10, pp. 2771-2784.

Vazquez, N., Lopez, H., Hernandez, C., Vazquez, E., Osorio, R. and Arau, J. (2009), "A different multilevel current-source inverter", *IEEE Transactions on Industrial Electronics*, Vol. 57 No. 8, pp. 2623-2632.

Wang, X., Loh, P.C. and Blaabjerg, F. (2017), "Stability analysis and controller synthesis for single-loop voltage-controlled VSIs", *IEEE Transactions on Power Electronics*, Vol. 32 No. 9, pp. 7394-7404.

Wang, X., Blaabjerg, F. and Loh, P.C. (2015), "High-performance feedback-type active damping of LCL-filtered voltage source converters", *2015 IEEE Energy Conversion Congress and Exposition (ECCE)*, *IEEE*, pp. 2629-2636.

Wang, X., Blaabjerg, F., Chen, Z. and Wu, W. (2013), "Resonance analysis in parallel voltage-controlled distributed generation inverters", *2013 Twenty-Eighth Annual IEEE Applied Power Electronics Conference and Exposition (APEC)*, *IEEE*, pp. 2977-2983.

Watanabe, H. and Itoh, J.I. (2015), "Novel DC to single-phase AC isolated current source inverter with power decoupling capability for micro-inverter system", *2015 IEEE Energy Conversion Congress and Exposition (ECCE)*, *IEEE*, pp. 158-165.

Wei, B., Guerrero, J.M., Vásquez, J.C. and Guo, X. (2016), "A modified droop control method for parallel-connected current source inverters", *IECON 2016-42nd Annual Conference of the IEEE Industrial Electronics Society*, *IEEE*, pp. 5195-5200.

Wiechmann, E.P., Aqueveque, P., Burgos, R. and Rodríguez, J. (2008), "On the efficiency of voltage source and current source inverters for high-power drives", *IEEE Transactions on Industrial Electronics*, Vol. 55 No. 4, pp. 1771-1782.

Wu, B., Pontt, J., Rodríguez, J., Bernet, S. and Kouro, S. (2008), "Current-source converter and cycloconverter topologies for industrial medium-voltage drives", *IEEE Transactions on Industrial Electronics*, Vol. 55 No. 7, pp. 2786-2797.

Yuan, G., Luo, S., Zhou, S., Zou, X. and Zou, K. (2015), "Low-order harmonics analysis and suppression method for 400Hz single-phase VSI", *2015 IEEE Applied Power Electronics Conference and Exposition (APEC)*, *IEEE*, pp. 2341-2345.

Zhao, X., Guerrero, J.M. and Wu, X. (2014), "Review of aircraft electric power systems and architectures", *2014 IEEE International Energy Conference (ENERGYCON)*, *IEEE*, pp. 949-953.

Zmood, D.N. and Holmes, D.G. (1998), "A generalised approach to the modulation of current source inverters", *PESC 98 Record. 29th Annual IEEE Power Electronics Specialists Conference (Cat. No. 98CH36196)*, Vol. 1, *IEEE*, pp. 739-745.

Zmood, D.N. and Holmes, D.G. (2001), "Improved voltage regulation for current-source inverters", *IEEE Transactions on Industry Applications*, Vol. 37 No. 4, pp. 1028-1036.

Further reading

Barbosa, P.G., Braga, H.A.C., Rodrigues, M.D.C.B. and Teixeira, E.C. (2006), "Boost current multilevel inverter and its application on single-phase grid-connected photovoltaic systems", *IEEE Transactions on Power Electronics*, Vol. 21 No. 4, pp. 1116-1124.

He, J., Zhang, D. and Torrey, D. (2018), "Recent advances of power electronics applications in more electric aircrafts", *2018 AIAA/IEEE Electric Aircraft Technologies Symposium (EATS)*, IEEE, pp. 1-8.

Loh, P.C., Vilathgamuwa, D.M., Lai, Y.S., Chua, G.T. and Li, Y. (2004), October. "Pulse-width modulation of Z-source inverters", *Conference Record of the 2004 IEEE Industry Applications Conference, 2004. 39th IAS Annual Meeting*, Vol. 1, *IEEE*.

Shen, M., Joseph, A., Wang, J., Peng, F.Z. and Adams, D.J. (2007), "Comparison of traditional inverters and Z -source inverter for fuel cell vehicles", *IEEE Transactions on Power Electronics*, Vol. 22 No. 4, pp. 1453-1463.

Wang, X., Li, Y.W., Blaabjerg, F. and Loh, P.C. (2014), "Virtual-impedance-based control for voltage-source and current-source converters", *IEEE Transactions on Power Electronics*, Vol. 30 No. 12, pp. 7019-7037.

Corresponding author

Eralp Sener can be contacted at: eralp.sener@bilecik.edu.tr